ABSTRACT

A Theoretical Study of the Subband Structures and Tunneling in Polytype Heterostructures

by
Hong Chen

A theoretical study of the electronic and optical properties in polytype heterostructures is presented in this thesis.

In the first part of the thesis (Chap. 2 and Chap. 3), an explicit expression for calculating the subband structure and tunneling is formulated by the incorporation of the envelope function approximations and the transfer matrix technique. It is based on the **k·p** theory as done to date, but contains two significant improvements: a more realistic treatment of the spatial and energetic dependance of effective masses and band edges; the availability of the calculations, in favor of direct numerical evaluation, to various quantum well structures composed of complicated bases.

The second part of the thesis is devoted to applications of the theoretical approach. A computer program written in Fortran-77 is used to calculate the subband structures and tunneling coefficients for various polytype quantum well structures. From such calculations, the feasibilities of quantum well infrared laser for some special designed structures are studied by considerations of population inversion and the different relaxation mechanisms of the carriers.

A THEORETICAL STUDY OF THE SUBBAND STRUCTURES AND TUNNELING IN POLYTYPE HETEROSTRUCTURES

by
Hong Chen

A Thesis
Submitted to the Faculty of New Jersey
Institute of Technology
in Partial Fulfillment of the Requirements for the Degree of
Master of Science
Department of Applied Physics
October, 1992

APPROVAL PAGE

A Theoretical Study of the Subband Structures and Tunneling in Polytype Heterostructures

by
Hong Chen

May 26, 1992

Dr. K. Ken Chin, Thesis Advisor
Associate Professor of Applied Physics, NJIT

May 26, 1992

Dr. John C. Hansel, Committee Member
Distinguished Research Professor of Physics, NJIT

May 26, 1992

Dr. William Savin, Committee Member
Professor of Physics, NJIT

BIOGRAPHICAL SKETCH

Author: Hong Chen

Degree: Master of Science in Applied Physics

Date: October, 1992

Date of Birth:

Place of Birth:

Undergraduate and Graduate Education:

Master of Science in Applied Physics, New Jersey Institute of Technology, Newark, NJ, 1992

Master of Science in Physics, Fudan University, Shanghai, The People's Republic of China, 1985

Bachelor of Science in Physics, Fudan University, Shanghai, The People's Republic of China, 1982

Major: Applied Physics

This thesis is dedicated to
my wife Yubei Wu

ACKNOWLEDGMENT

The author wishes to express his sincere gratitude to his advisor, Dr. K. Ken Chin, for his guidance throughout this research.

Special thanks to Professors John C. Hansel and William Savin for serving as members of the committee.

The author is grateful to Prof. Guanhua Feng for his resourceful suggestions and discussions in the structure design, Mr. Guang Yang and Mr. Ganmin Qin for their assistance in the preparation of numerical results. And the author is also thankful to all his colleagues for providing an intellectually stimulating and enjoyable environment.

Finally, the author would like to express his appreciation to his wife Yubei Wu for her consistent assistance in many ways in the past years. The author deeply appreciates the endless love of his family and his family-friend, Dr. Shun Chen who support him and encourage him so much during his study in the Unite State of American.

TABLE OF CONTENTS

Page

LIST OF TABLES

LIST OF FIGURES

CHAPTER 1
INTRODUCTION

Recently advances in microstructure technology in semiconductors like molecular beam epitaxy (MBE) and electron beam lithography have made ultrathin and ultrasmall novel structures possible. Among these, the electronic and optical properties of the superlattice and quantum well have been extensively studied because of their interesting physical phenomena and possible device applications.

Up to date, a wide range of quantum well systems has been grown and studied. Established epitaxial growth techniques are capable of growing many new systems that have not yet been investigated. Because of different types of band-edge lineups, various materials systems can show qualitatively different physical behaviors. The electronic structure of a superlattice or quantum well depends on the layer thickness as well as on the constituent materials. The precise controllability of the layer thickness allows us to design the electron band structure of semiconducting materials. Moreover, we also design a novel structure for a special device.

This thesis serves two principal purposes. The first is to develop a useful theoretical description and calculation approach for the electronic and optical properties of superlattice and quantum well. With an increasing interest in applications of novel quantum well structures, an accurate but simple calculation model is necessary for the theoretical predictions and explanations of experimental results as well as the design of device structures. The theoretical approach is based on the envelope function approximation within the $\mathbf{k}\cdot\mathbf{p}$ theory scheme (in Chapter 2). The envelope function equations are solved by the transfer matrix technique (in Chapter 3). An explicit expression of tunneling coefficient and subband structure for various quantum well structures are also given in Chapter 3.

The second principal purpose of the thesis is to apply the model of calculation to practical device structures. The numerical results of such calculations are presented in Chapter 4. As a special application of the calculations, the feasibility study of the quantum well infrared laser is demonstrated.

In my view, one of the most interesting challenges in physics of semiconductor superlattice and quantum well is to utilize the power of modern epitaxial growth techniques by inventing new physical structures that show interesting and technologically important new properties. An accurate and simple theory plays an important role in the challenge.

CHAPTER 2
ENVELOPE-FUNCTION APPROXIMATION

2.1 Introduction

Theory of Electronic structure has a unique role to play in superlattice and quantum well research because of the rich variety of possible material systems. The theory can be used to invent structure that exhibit new physical phenomena. In some cases these phenomena have technological applications. Theory can also be used to tailor superlattice electronic structure either to enhance the observation of a particular effect or to optimize the material for a technological purpose.

There is an essential difference between the role of electronic-structure theory in superlattice research and that in conventional semiconductors. For conventional semiconductors, theory can be used to describe the electronic structure and to interpret experiments that depend on the electron structure. There are, however, few parameters available for designing new material. The large number of potential superlattice systems allows great freedom in material design. Theory can play an important role in this design process, which is sometimes called bandgap engineering.

The energy offsets between corresponding bands in the constituent materials of a superlattice are typically on the order of a few hundred mev; modifications in the electronic structure due to the periodic superlattice potential are on this energy scale. Thus a theoretical description of superlattice electronic structure must deal with questions on this energy scale. Those electronic states whose mean free path is comparable to or longer than the thickness of the constituent material layers are significantly influenced by the spatial modulation of the superlattice. States whose mean free path is much less than the thickness of the constituent material layers are essentially kinetically confined within a particular material. Such states, therefore, are not modified greatly by superlattice modulation. As a result, electronic states relatively close in energy to band edges, which have relatively long lifetimes and mean free paths, are of greatest interest in superlattice material. Thus, theories of superlattice electronic structure are band-edge theories.

A very wide range of theoretical techniques has been applied to superlattice electronic-structure calculation. The degree of complexity in these approaches ranges from scaled Kronig-Penney models to self-consistent many-electron calculations. Which theoretical approach is most appropriate depends on the material system studied and the questions asked about that material system.

For the purpose of device design, the envelope-function approach based on $\mathbf{k}\cdot\mathbf{p}$ theory has proved efficient, relatively reliable as compared with more sophisticated approaches, and has the merit of often leading to analytical results.

Starting from Kane's $\mathbf{k}\cdot\mathbf{p}$ theory in Section 2. 2, we shall rederive envelope-function equations, which indicate nonparabolicity and the fact that the constituent materials have different bulk effective mass with three-band models in Section 2. 3. This Schrodinger-like equation with appropriate boundary conditions fulfilled by the envelope-function at the interface will be a fundamental tool of describing electronic-structure in superlattices and quantum wells. It gives dispersion relations for a wave vector along the growth axis and energy subbands in superlattice. It can also be used for calculations of transmission mechanism and optical properties.

2.2 Kane's k·p Theory [1]

In bulk semiconductor, $\mathbf{k}\cdot\mathbf{p}$ theory is particularly effective at describing states near the conduction- and valence-bands edges. As mentioned above, it is the band-edge states of superlattices that are of primary interest. For this reason, it is natural to consider $\mathbf{k}\cdot\mathbf{p}$ methods for describing these states in superlattices. The first theoretical efforts to describe superlattices based on Kronig-Penney models had considerable success in describing the optical properties of GaAs/Ga1-xAlxAs superlattices. The currently developed theoretical methods which can account for much more effects also utilize the **k·p** scheme.

2.2.1 The k·p Representation

In the one-electron problem of an electron moving in a periodic potential V(**r**), the eigenvalue equation for the electron energy E is

$$H\ \Psi = \left\{ \frac{p^2}{2m_0} + V(r) \right\} \Psi = E\ \Psi \tag{1.1}$$

Bloch showed that Ψ may be written

$$\Psi = \exp(i\,k \cdot r)\ U_{nk}(r) \tag{1.2}$$

where $U_{nk}(r)$ has the periodicity of V(**r**), and k lies in the first Brillouin zone and n is a band index running over a complete set of bands. Substituting Eq.(1.2) in Eq.(1.1) gives

$$\left\{ \frac{p^2}{2m_0} + \frac{\hbar}{m_0}(k \cdot p) + \frac{\hbar^2 k^2}{2m_0} + V(r) \right\} U_{nk}(r) = E_n(k)\, U_{nk}(r) \tag{1.3}$$

For any given **k**, the set of all $U_{nk}(r)$ is complete for functions having the periodicity of V(**r**). Hence if we choose $\mathbf{k} = \mathbf{k}_0$, the wave function for any **k** may be expressed in terms of the wave function for $\mathbf{k}_0$,

$$U_{nk}(r) = \sum_m C_{nm}(k - k_0)\ U_{mk_0}(r) \tag{1.4}$$

We call this the $\mathbf{k}_0$ representation.

We define H_{k_0} to be

$$H_{k_0} = \frac{p^2}{2m_0} + \frac{\hbar}{m_0}(k_0 \cdot p) + \frac{\hbar^2 k_0^2}{2m_0} + V(r) \tag{1.5}$$

then, by the above discussion,

$$H_{k_0} U_{nk_0} = E_n(k_0) U_{nk_0} \tag{1.6}$$

$$\left\{ H_{k_0} + \frac{\hbar}{m_0}(\mathbf{k} - \mathbf{k}_0) \cdot \mathbf{p} + \frac{\hbar^2}{2m_0}(k^2 - k_0^2) \right\} U_{nk} = E_n(\mathbf{k}) U_{nk} \tag{1.7}$$

We can easily convert Eq.(1.7) to a matrix eigenvalue equation by substituting Eq.(1.4) in Eq.(1.7), multiplying both sides of Eq.(1.7) by $U_{nk}(r)$, and integrating over the unit cell in which the U's are normalized:

$$\sum_m \left\{ \left(E_n(k_0) + \frac{\hbar^2}{2m_0}(k^2 - k_0^2) \right) \delta_{nm} + \frac{\hbar}{2m_0}(k - k_0) \cdot P_{nm} \right\} C_{nm}$$

$$= E_n(k) C_{nm} \tag{1.8}$$

$$P_{nm} = \int_{\text{unit cell}} U^*_{nk_0}(r) \; \mathbf{p} \; U_{nk_0}(r) \; dr \tag{1.9}$$

Equation (1.8) is the eigenvalue equation for the point **k** written in the $\mathbf{k}_0$ representation.

Although Eq.(1.8) as it stands is correct for any **k**, it is most useful when **k** is near $\mathbf{k}_0$ so that the nondiagonal part of the Hamiltonian

$$\frac{\hbar}{m_0}(k - k_0) \cdot P_{nm} \tag{1.10}$$

can be treated as a perturbation.

In the case of a single band treated by ordinary perturbation theory, Eq.(1.8) gives, for the energy in the neighborhood of $\mathbf{k}_0$ to second order,

$$E_n(k) = E_n(k_0) + \frac{\hbar}{m_0}(k-k_0)\cdot P_{nm} + \frac{\hbar^2}{2m_0}(k^2-k_0^2)$$
$$+ \frac{\hbar^2}{m_0^2}\sum_m \frac{|i\cdot P_{nm}|^2}{E_n(k_0)-E_m(k_0)} \quad (1.11)$$

The expansion point $\mathbf{k}_0$ is frequently an extreme so that $\mathbf{P}_{nn}+\hbar\mathbf{k}_0 = 0$. Assuming $\mathbf{k}_0$ is an extreme and using principal axes, Eq.(1.11) becomes

$$E_n(k) = E_n(k_0) + \frac{\hbar^2}{2}\sum_{i=1}^{3}\frac{(k_i-k_{0i})^2}{m_i^*} \quad (1.12)$$

$$\frac{1}{m_i^*} = \frac{1}{m_0} + \frac{2}{m_0^2}\sum_m \frac{|i\cdot P_{nm}|^2}{E_n(k_0)-E_m(k_0)} \quad (1.13)$$

where **i** is a unit vector in the direction of the ith principal axes and mm the effective mass. Eq.(1.12) are dispersion relations, which in the vicinity of an edge located at $\mathbf{k}_0$ are parabolic in terms of ($\mathbf{k}$ - $\mathbf{k}_0$).

Refinements can be included within the $\mathbf{k}\cdot\mathbf{p}$ method to account for departures from quadratic dispersion relations (the band nonparabolicity) when the kinetic energy in the nth band, $E_n(k)-E_n(k_0)$ is not very small compared with the $\mathbf{k}_0$ band gaps $E_n(k_0)-E_m(k_0)$. This, of course, happens more often in narrower-band-gap semiconductors(e.g. InSb, InAs, Hg1-xCdxTe).

2.2.2 Kane's Model

The Kane model is the most commonly used to account for nonparabolicity effects. For Zincblende III-V and II-VI materials, the fundamental band gap occurs at the point(k=0, see Fig. 1.1). The Kane model is an exact diagonalization of the ($\hbar$/m)$\mathbf{k}\cdot\mathbf{p}$ perturbation in the(truncated) basis generated by the eight zone center Bloch functions of the conduction band(2), topmost valence band(4) and split-off valence band(2):

$$H_{no}\, U_{no} = E_n(0)\, U_{no} \tag{1.14}$$

where H_{no} is the Hamiltonian including spin orbit interactions, U_{no} are the eigenfunctions with eigenvalues $E_n(0)$. These wave functions and corresponding eigenvalues are listed in Table 1.1, where s, x, y, z denote periodic functions that transform like s, x, y, z atomic functions under the symmetry operations that map the local tetrahedron onto itself.

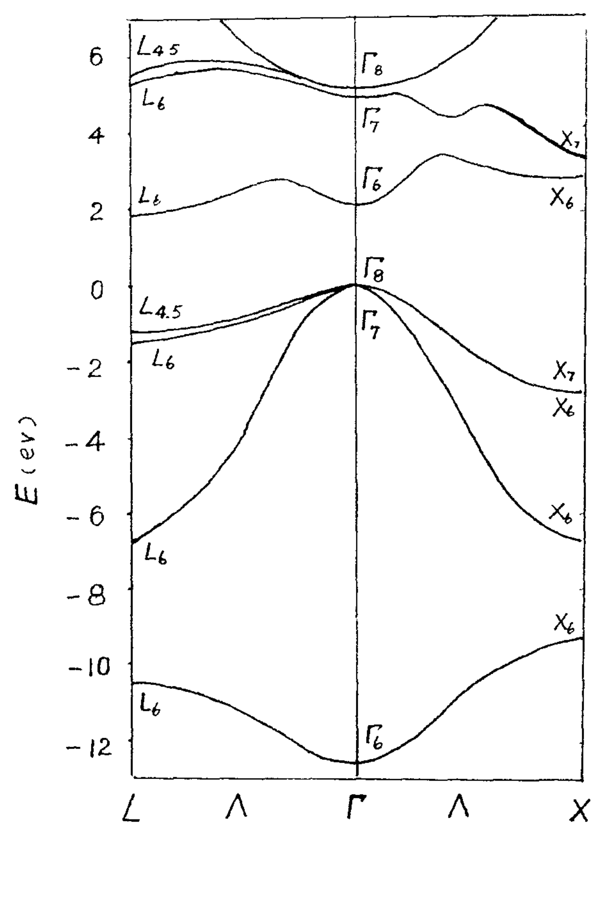

Figure 1.1 Band Structure of A Direct III-V Compound (e.g., GaAs) in the Vicinity of the Center of the Brillouin Zone

TABLE 1.1

Periodic Parts of the Bloch Functions at the Γ_6, Γ_7, Γ_8 Edges. l Denotes the Orbital Angular Momentum, j the Total Angular Momentum and m Its Quantized Projection along Growth Axis.

U_{n0} $\|l,j,m>$	U_{jm}	E(k=0)
$U_{10} = \|s,1/2,1/2>$	$= \|i s>$	0
$U_{30} = \|p,3/2,3/2>$	$=\sqrt{1/2}\|(x+iy)>$	$-E_0$
$U_{50} = \|p,3/2,1/2>$	$= -\sqrt{2/3}\|z> +\sqrt{1/6}\|(x+iy)>$	$-E_0$
$U_{70} = \|p,1/2,1/2>$	$=\sqrt{1/3}\|(x+iy)> +\sqrt{1/3}\|z>$	$-E_0-\Delta$
$U_{20} = \|s,1/2,-1/2>$	$= \|i s>$	0
$U_{40} = \|p,3/2,-3/2>$	$=\sqrt{1/2}\|(x-iy)>$	$-E_0$
$U_{60} = \|p,3/2,-1/2>$	$= -\sqrt{2/3}\|z> -\sqrt{1/6}\|(x-iy)>$	$-E_0$
$U_{80} = \|p,1/2,-1/2>$	$= -\sqrt{1/3}\|(x-iy)> +\sqrt{1/3}\|z>$	$-E_0-\Delta$

Following the process of degenerate perturbation theory, we can find the matrix eigenvalue equation:

$$\sum_{m} \left\{ E_n(0)\,\delta_{nm} + \frac{\hbar}{m_0} k \cdot P_{nm} \right\} C_{nm} = E_n(k)\,C_{nm} \tag{1.15}$$

where the matrix elements of $\frac{\hbar}{m_0} k \cdot P_{nm}$ are listed in Table 1.2.

TABLE 1.2 the Matrix Elements of $\frac{\hbar}{m_0} k \cdot P_{nm}$

Un0	U10	U30	U50	U70	U20	U40	U60	U80
U10	0	0	$\sqrt{\frac{2}{3}}\hbar pk$	$\sqrt{\frac{1}{3}}\hbar pk$	0	0	0	0
U30	0	$-E_0$	0	0	0	0	0	0
U50	$\sqrt{\frac{2}{3}}\hbar pk$	0	$-E_0$	0	0	0	0	0
U70	$\sqrt{\frac{1}{3}}\hbar pk$	0	0	$-E_0-\Delta$	0	0	0	0
U20	0	0	0	0	0	0	$\sqrt{\frac{2}{3}}\hbar pk$	$\sqrt{\frac{1}{3}}\hbar pk$
U40	0	0	0	0	0	$-E_0$	0	0
U60	0	0	0	0	$\sqrt{\frac{2}{3}}\hbar pk$	0	$-E_0$	0
U80	0	0	0	0	$\sqrt{\frac{1}{3}}\hbar pk$	0	0	$-E_0-\Delta$

The dispersion relations are each fund to be doubly degenerate and the solutions of

$$\lambda (\lambda + E_0) (\lambda + E_0 + \Delta) = p^2\hbar^2k^2(\lambda + E_0 + \tfrac{2}{3}\Delta) \quad (1.16a)$$

$$\lambda = -E_0 \quad (1.16b)$$

where

$$\lambda = E - \frac{\hbar^2k^2}{2m_0} \quad (1.17)$$

In Eqs.(1.16) the energy origin is taken at the Γ_6 (s-like) edge, $E_0 = E_6 - E_8$ is the fundamental band gap, $\Delta = E_8 - E_7$ is the zone center spin-orbit coupling, and

$$p = -\frac{i}{m_0}<s \mid p_x \mid x> \quad (1.18)$$

is the Kane matrix element between the conduction band $|s>$ and the valence band $|p>$. For GaAs, $2\, m_0P^2 = 21.5$ ev [8].

2.2.3 Effective Mass Equation

From Eq.(1.15), a Schrodinger-like equation related to Γ_6 can be obtained:

$$\left(P \frac{1}{m^*_{\Gamma_6}} P \right) f = E f \quad (1.19)$$

where the Γ_6 effective mass $m^*_{\Gamma_6}$ is isotropic and is such that

$$\frac{1}{m^*_{\Gamma_6}} = \frac{1}{m_0} + \frac{2p^2(E_0 + \frac{2}{3}\Delta)}{E_0(E_0 + \Delta)} \quad (1.20)$$

where usually the second term dominates the free-electron one. Eq.(1.20) reciprocally allow a determination of P if $m^*_{\Gamma_6}$, E_0 and Δ are known, which is usually the case.

2.3 The Envelope Function Scheme [4-10]

We shall discuss the electronic states found in heterostructures made out of lattice-matched semiconductors. Modern expitaxy techniques(MBE, MOCVD) allow in principle the growth of defect-free, atomically sharp interfaces between two lattice-matched homopolar semiconductors(e.g. III-V on III-V or II-VI on II-VI), thus an idea interface between an AC semiconductor and BC semiconductor will be a plane of C atoms. Each of the host materials has a band structure characterized by dispersion relations $E_n(k_A)$, $E_n(k_B)$ and Bloch functions $\Psi^{(A)}_{nk_A}(r)$, $\Psi^{(B)}_{nk_B}(r)$. For allowed energies, the wave functions $\Psi^{(A)}_{nk_A}(r)$ and $\Psi^{(B)}_{nk_B}(r)$ display the familiar form:

$$\Psi^{(A)}_{nk_A}(r) = \frac{1}{\sqrt{\Omega}} \exp(i\, k_A \cdot r)\, U_{nk_A}(r) \tag{1.21}$$

where U_{nk_A} is a periodic function and $\mathbf{k}_A$ is a real wave vector that can be restricted to the first Brillouin zone of the A material. An expression similar to Eq.(1.21) holds for the B Material.

It may be noted that there is a difference between bulk semiconductors and heterostructures. No propagating bulk states exists in the forbidden gaps separating the allowed energy $E_n(k_A)$ and $E_n(k_B)$. However, since layers of finite thickness along z (L_A, L_B, respectively) are involved in heterostructures, one must also retain the host evanescent states, whose energies fall in the bulk forbidden gaps. To illustrate this point, one may consider the U_n's equal to unity in Eq.(1.21), and take the energy zero at the top of the quantum well. To calculate the allowed bound energy levels (E<0) of this model heterostructure, we have to find the bulk propagating and evanescent states in each kind of layer. Inside the well, these are plane waves with real wave vectors of opposite signs. Outside the well there are also plane waves but with imaginary wave vectors, i.e., evanescent states with exponentially growing or decaying wave functions(see Fig. 1.2).

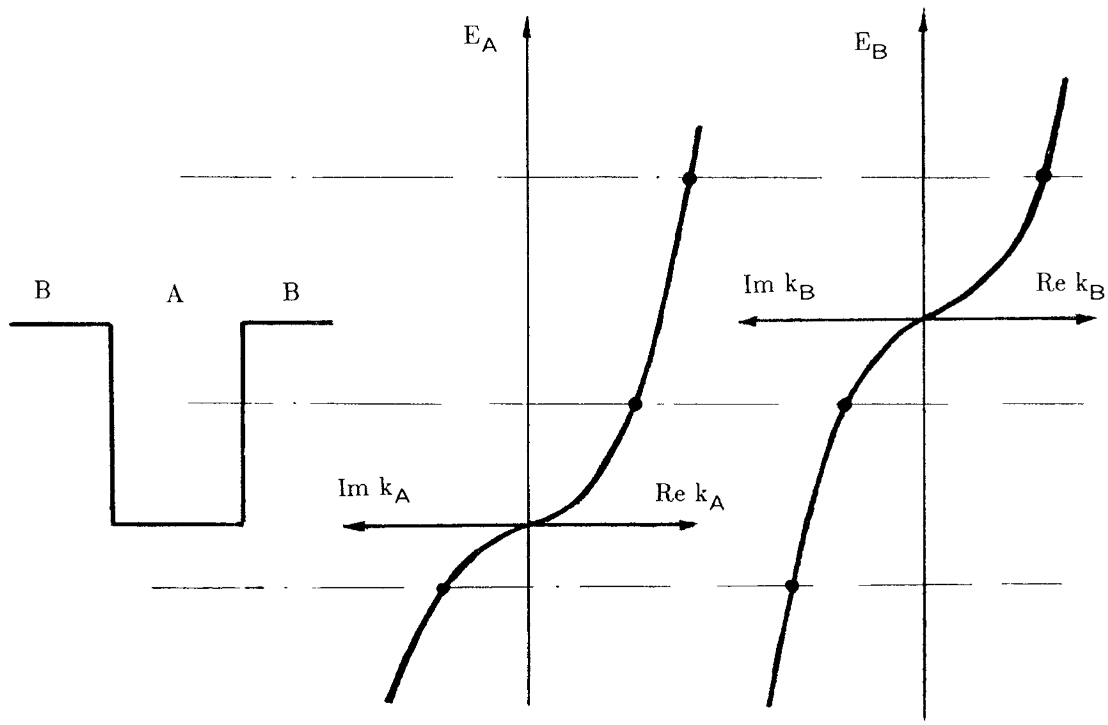

Figure 1.2 Dispersion Relations upon the Real and Imaginary Wave Vectors in A and B Layers Stacked to Form a BAB Quantum Well.

2.3.1 Building Heterostructure States

In actual semiconductor heterostructures, we shall proceed exactly in the same way as outlined for textbook quantum wells. For a given energy E wave function in the A and B layers can be expanded in terms of the complete orthonormal set of bulk eigenstates,

$$\Phi(\mathrm{r}) = \begin{cases} \sum\limits_{n,\, k_A} C_n^{(A)}(k_n^{(A)})\, \Psi_{nk_A}^{(A)}(\mathrm{r}) & z \in B \\ \sum\limits_{n,\, k_B} C_n^{(B)}(k_n^{(B)})\, \Psi_{nk_B}^{(B)}(\mathrm{r}) & z \in B \end{cases} \tag{1.22}$$

In Eq. (1.22) the summation runs over all the bands of A and B host layers; $k_n^{(A)}, k_n^{(B)}$ are the propagating (or evanescent) wave vectors solutions of the implicit equations,

$$E_n^{(A)}(k_n^{(A)}) = E \quad , \qquad E_n^{(B)}(k_n^{(B)}) = E \tag{1.23}$$

and $\Psi_{nk_A}^{(A)}(\mathrm{r})$, and $\Psi_{nk_B}^{(B)}(\mathrm{r})$, are the Bloch functions for the nth band and wave vector **k**. The coefficients $C_n^{(A)}$and $C_n^{(B)}$are determined by imposing the boundary condition: the continuity of Φ and $\frac{\partial\Phi}{\partial z}$ across the interfaces. For instance, in a superlattice structure we require HHH to satisfy the Bloch theorem:

$$\Phi(\rho,\ z+d) = \exp(i\, q\, d)\, \Phi(\rho,\ z) \tag{1.24}$$

In a quantum box we require that $\Phi(\mathrm{r}) \rightarrow 0$ far away from the box, and so forth.

The general solutions given in Eq.(1.22) is totally useless because the Bloch functions are seldom known for all the bands of a crystal. Thus we need to truncate the summation in Eq. (1.22) by using some physical reasoning.

The key remarks on which envelope function type of models are based are

(a). Most of host materials display similar band structures. Moreover, the periodic parts of the Bloch functions of the relevant band edges do not differ very much from one host material to the other.

(b). The relevant electronic states of the actual heterostructure are often close from the band extrema of the hosts. Thus, only a small fraction of the host Brillouin zone participates in the building of the heterostructure states. It is a fair approximation to take only the Γ_6, Γ_7, Γ_8 edges into consideration to build the quantum well states in this energy range.

In addition, we shall assume that the host materials are lattice-matched, and that flat band conditions are satisfied.

The remark (a) means that the zone center periodic parts of the Bloch functions are the same in the A and B layers:

$$U_{n0}^{(A)}(\mathbf{r}) = U_{n0}^{(B)}(\mathbf{r}) = U_{n0}(\mathbf{r}) \tag{1.25}$$

This identity is, of course, not exactly true, but it is very reasonable in view of, for example, the constancy of the Kane matrix elements $\langle s|P_X|p\rangle$ across the III-V or II-VI family.

The remark (b) implies that the envelope function scheme is a band-edge theory. In many III-V or II-VI based heterostructures, the band edges relevant to optical and transport properties have the Γ_6, Γ_7, Γ_8 symmetries. Thus, the states whose energies relatively close to the Γ points in both layers will be described in terms of the $\mathbf{k}\cdot\mathbf{p}$ expansion around the Γ point. As a result, the summation in Eq.(1.22) runs over all the host band edges but Γ_6, Γ_7, Γ_8

For heterostructures with a unidirectional modulation(z-axis) and under flat-band conditions, we can exploit the translational invariance in the layer plane to assert that the in-plane projection of the electron wave vector

$$\mathbf{k}_{\perp} = (k_x, k_y) \tag{1.26}$$

is a good quantum number. Hence

$$k_n^{(A)} = (k_\perp , k_{nz}^{(A)})$$

$$k_n^{(B)} = (k_\perp , k_{nz}^{(B)}) \qquad (1.27)$$

The above discussion with respect to Eqs. (1.25)--(1.27) allows us to rewrite Equation (1.22) in the simple form

$$\Phi(\mathbf{r}) = \exp (i \mathbf{k}_\perp \cdot \mathbf{r}) \sum_{n=1}^{8} U_{no}(\mathbf{r}) f_n^{(A,B)}(z) \quad (27) \qquad (1.28)$$

where $f_n(z)$ is an envelope function that is slowly varying on the scale of the host periodicity. If, as assumed so far, there is no band bending in the heterostructures, f_n is a linear combination of plane waves,

$$f_n^{(A,B)}(z) = \frac{1}{\sqrt{\Omega}} \sum_{k_z} C_n^{(A,B)}(k_z^{(A,B)}) \exp(ik_z \cdot z) \quad . \qquad (1.29)$$

We can see from Eq. (1.28)--(1.29) that the wave function $\Phi(\mathbf{r})$ is a sum of products of slowly varying functions at the scale of the host unit cell (the envelope functions) $f_n(z)$ by band edge periodic functions $U_{no}(\mathbf{r})$. It is the clear cut separation between the spatial extensions of the two kinds of terms which underlie the envelope function scheme. The rapidly varying terms will later enter in the heterostructure calculation only through effective parameters. Together with the host crystalline potentials, the fixed band gap, interband P matrix elements, etc. All these quantities are assumed to be a priori known in the envelope function approximation. The slow spatial variations will be taken more exactly into account: our goal is to find a Schrodinger-like equation governing their spatial behaviors. This equation will be parametrized by effective parameters, which are remnant of the host material periodicities, and will not in general be a scalar since several host band edges may participate in the building of the f_n wave function.

2.3.2 The Effective Hamiltonian

Let us now establish the effective Hamiltonian acting on the envelope function. To do so, we write the Hamiltonian in the form

$$H = \frac{p^2}{2m_0} + V_A(r)\,\Theta(z \in A) + V_B(r)\,\Theta(z \in B) + V_{ext}(z), \tag{1.30}$$

Where the function $\Theta(z \in B)$ [is introduced

$$\Theta(z \in Q) = \begin{cases} 1 & z \in Q \\ 0 & \text{otherwise} \end{cases}, \qquad Q = A, B. \tag{1.31}$$

In Eq.(1.30) $V_{ext}(z)$ is the external potential, assumed to depend only on the z coordinate, and . The Uno are, by definition, solutions of

$$\left(\frac{p^2}{2m_0} + V_{(A,B)}(r) \right) U_{no}(r) = E_n^{(A,B)}(0)\, U_{no}(r). \tag{1.32}$$

Letting H act on Eq.(1.28)

$$H\,\Phi(r) = \left\{ \frac{p^2}{2m_0} + V_A(r)\,\Theta(z \in A) + V_B(r)\,\Theta(z \in B) + V_{ext}(z) \right\}$$

$$\cdot \left\{ \exp(i\,k_\perp \cdot r) \sum_{n=1}^{8} U_{no}(r)\, f_n^{(A,B)}(z) \right\}$$

$$= E \left\{ \exp(i\,k_\perp \cdot r) \sum_{n=1}^{8} U_{no}(r)\, f_n^{(A,B)}(z) \right\}, \tag{1.33}$$

multiplying $.U_{mo}$, integrating over a unit cell, and making use of the different length of variations of the envelope function f_n and the cell periodic parts, we finally get

$$D \cdot f \;=\; E\, f \tag{1.34}$$

where **f** is an 8 x 1 column vector whose components f_n are solutions of the coupling differential system:

$$\left\{ E_n^{(A)}(0)\ \Theta(z \in A) + E_n^{(B)}(0)\ \Theta(z \in B) + V_{ext}(z) + \frac{\hbar^2 k_\perp{}^2}{2m_0} - \frac{\hbar^2}{m_0}\frac{d^2}{dz^2} \right\} f_n(z)$$

$$+ \sum_{n=1}^{8} \left\{ \frac{\hbar}{m_0}\, k_\perp \cdot < U_{n0} | P_\perp | U_{m0} > + \frac{1}{m_0} < U_{n0} | p_z | U_{m0} > \frac{1}{i}\frac{d}{dz} \right\} f_m(z)$$

$$= E\, f_n(z) \tag{1.35}$$

D is thus the effective Hamiltonian we were looking for. All the microscopic information about the rapidly varying function has explicitly disappeared from D. It survives, however, through effective parameters such as the band gaps and the Kane matrix elements. Notice also that in the envelope function Hamiltonian the potential steps at the interface $E_n^{(B)}$- $E_n^{(A)}$appear only in the diagonal. This results from the assumption Eq.(1.25) and is more related to a symmetry argument than to an assumption of a slow variation.

The energy E of the electronic state under consideration is related to khh, khh, khh, by the two relations

$$E \;=\; E(\, k_\perp\, ,\ k_z^{(A)}) \ ; \qquad E \;=\; E(\, k_\perp\, ,\ k_z^{(B)}) \tag{1.36}$$

Let us take the A material as a reference for the energy scale, then, E and **k** , are univoquely related by means of the dispersion relations of the bulk A layer. A crucial point in evaluating **k** is the band lineup of the A and B materials at the heterointerface:

$$E_n^{(A)}(0)\ \Theta(z\in A) + E_n^{(B)}(0)\ \Theta(z\in B) = E_n^{(A)} + V_n(z), \tag{1.37}$$

where V_n are step functions

$$V_n(z) = \begin{cases} 0, & \text{when } z \in A \\ E_n^{(B)}(0) - E_n^{(A)}(0), & \text{when } z \in B \end{cases} \tag{1.38}$$

Thus, they are the algebraic energy shifts of the nth edge when going from the A layer to the B layer. If E_A, E_B, Δ_A, Δ_B are the Γ_6--Γ_8 band-gaps and zone center spin orbit coupling in the A and B layers, respectively, there exists a single unknown, say the Γ_6 offset (hereafter termed Vs),[11-15] and the other edge offsets (V_p and V_δ, respectively) are expressible in terms of V_s, E_A, E_B, Δ_A, Δ_B (see Fig. 1.3)

$$E_A - V_p = E_B - V_s \tag{1.39}$$

$$\Delta_A = \Delta_B - V_p + V_\delta \tag{1.40}$$

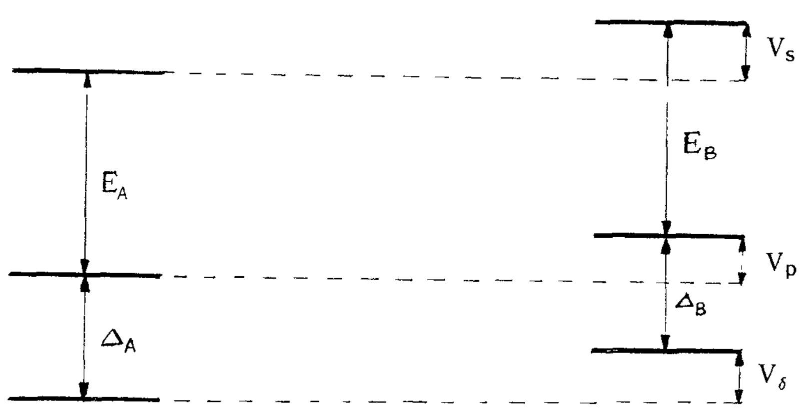

Figure 1.3 Relation between Vs, Vp, V_δ, and E_A, E_B, Δ_A, Δ_B

The D_{nm} matrix elements can be explicitly evaluated from Eq.(1.35) and Table 1.1 and 1.2. One finds

$$\begin{bmatrix}
\zeta+V_s & p\hbar k_+ & -\sqrt{\frac{2}{3}}p\hbar k_z & \sqrt{\frac{1}{3}}p\hbar k_z & 0 & 0 & -\sqrt{\frac{1}{3}}p\hbar k_- & -\sqrt{\frac{2}{3}}p\hbar k_- \\
p\hbar k_- & \zeta-E_A+V_p & 0 & 0 & 0 & 0 & 0 & 0 \\
-\sqrt{\frac{2}{3}}p\hbar k_z & 0 & \zeta-E_A+V_p & 0 & \sqrt{\frac{1}{3}}p\hbar k_- & 0 & 0 & 0 \\
\sqrt{\frac{1}{3}}p\hbar k_z & 0 & 0 & \zeta-E_A-\Delta_A+V_\delta & \sqrt{\frac{2}{3}}p\hbar k_- & 0 & 0 & 0 \\
0 & 0 & \sqrt{\frac{1}{3}}p\hbar k_+ & \sqrt{\frac{2}{3}}p\hbar k_+ & \zeta+V_s & p\hbar k_- & -\sqrt{\frac{2}{3}}p\hbar k_z & \sqrt{\frac{1}{3}}p\hbar k_z \\
0 & 0 & 0 & 0 & p\hbar k_+ & \zeta-E_A+V_p & 0 & 0 \\
-\sqrt{\frac{1}{3}}p\hbar k_+ & 0 & 0 & 0 & -\sqrt{\frac{2}{3}}p\hbar k_z & 0 & \zeta-E_A+V_p & 0 \\
-\sqrt{\frac{2}{3}}p\hbar k_+ & 0 & 0 & 0 & \sqrt{\frac{1}{3}}p\hbar k_z & 0 & 0 & \zeta-E_A-\Delta_A+V_\delta
\end{bmatrix}$$

where the energy zero has been taken at the HH6 edge of the A material,

$$\zeta = \frac{\hbar^2 k^2}{2m_0} + V_{ext}(z) \tag{1.41a}$$

$$k_\pm = \sqrt{\tfrac{1}{2}}\,(k_x \pm i k_y) \tag{1.41b}$$

$$k = \left(k_\perp \, , \; -i\frac{\partial}{\partial z} \right) \tag{1.42}$$

and P is the Kane matrix element defined in Eq.(1.18).

Equation (1.35) is useful in order to calculate the Γ_6-related dispersion relation of heterostructures as well as the edges ($k = 0$) of the Γ_7- and Γ_8-($J_z=+1/2$)-related states. It has, however, a severe drawback, namely the inaccurate description of the heavy hole-related states and more generally of the Γ_8-Γ_7 kinematics.

2.3.3 Envelope Function Equation

If the in-plane wave vector is set equal to zero,

$$\mathbf{k}_\perp = 0, \tag{1.43}$$

a considerable simplification occurs: an inspection of Eqs.(1.40)–(1.43) reveals that:

(i) The f_n's associated with the heavy hole band edges |p,3/2,+3/2> become decoupled from those associate with the light hole band edges |s,1/2,+1/2>, |p,3/2,+1/2>, |p,1/2,+1/2>.

(ii) The eigenstates are twice degenerate.

Indeed the complete effective Hamiltonian Eq.(1.38) splits into decoupled and identical blocks:

$$D = \begin{bmatrix} D_+ & 0 \\ 0 & D_- \end{bmatrix} \tag{1.44}$$

where

$$D_\pm = \begin{bmatrix} \zeta+V_s & p\hbar k_+ & -\sqrt{\frac{2}{3}}p\hbar k_z & \sqrt{\frac{1}{3}}p\hbar k_z \\ p\hbar k_- & \zeta-E_A+V_p & 0 & 0 \\ -\sqrt{\frac{2}{3}}p\hbar k_z & 0 & \zeta-E_A+V_p & 0 \\ \sqrt{\frac{1}{3}}p\hbar k_z & 0 & 0 & \zeta-E-\Delta+V \end{bmatrix} \tag{1.45}$$

The second row and second column, which are uncoupled with the others, refer to the heavy hole states. The first row and column are associated with the Γ_6 edge, while the third and fourth rows and column refer to the |p,3/2,+1/2> and

|p,1/2,+1/2> edges, respectively.

The eigenstates at $\mathbf{k}_\perp = 0$ also split into two categories:

$$f = \begin{bmatrix} f_+ \\ f_- \end{bmatrix} \tag{1.46}$$

where $\mathbf{f}_+$ and $\mathbf{f}_-$ are now 4 x 1 column vectors that are, respectively, eigenstates of D_+ and D_-. The notations"+" and "-" represent the states with spin up and down.

To find a Schrodinger-like equation for envelope function related to Γ_6 light particle band edges, we remove the terms associated with the heavy hole band edge from Eq. (1.45), and then, we get

$$\begin{bmatrix} \zeta + V_s & -\sqrt{\frac{2}{3}}p\hbar k_z & \sqrt{\frac{1}{3}}p\hbar k_z \\ -\sqrt{\frac{2}{3}}p\hbar k_z & \zeta - E_A + V_p & 0 \\ \sqrt{\frac{1}{3}}p\hbar k_z & 0 & \zeta - E_A - \Delta_A + V_\delta \end{bmatrix} \begin{bmatrix} f_s \\ f_p \\ f_\delta \end{bmatrix} = E \begin{bmatrix} f_s \\ f_p \\ f_\delta \end{bmatrix} \tag{1.47}$$

or, more explicitly,

$$(\zeta + V_s) f_s - \sqrt{\frac{2}{3}}p\hbar k_z \; f_p + \sqrt{\frac{1}{3}}p\hbar k_z \; f_\delta = E f_s \quad , \tag{1.47a}$$

$$-\sqrt{\frac{2}{3}}p\hbar k_z \; f_s + (\zeta - E_A + V_p) \; f_p = E f_p \quad , \tag{1.47b}$$

$$\sqrt{\frac{1}{3}}p\hbar k_z \; f_s + (\zeta - E_A - \Delta_A + V_\delta) \; f_\delta = E f_\delta \tag{1.47c}$$

where the envelope function f_s, f_p and f_δ are associated with the conduction electron band edge |s,+1/2>, the valence light hole band edges |p,3/2,+1/2> and

$|p,1/2,+1/2>$, respectively.

From Eqs. (1.47b)-(1.47c), one may find f_δ and f_p in terms of f_s

$$f_p = \frac{-\sqrt{\frac{2}{3}}p\hbar k_z}{(\zeta - E_A + V_p)} f_s \tag{1.48}$$

$$f_\delta = \frac{-\sqrt{\frac{1}{3}}p\hbar k_z}{(\zeta - E_A - \Delta_A + V_\delta)} f_s \tag{1.49}$$

Substituting these into Eq. (1.47a) gives

$$[\ P_z \frac{1}{2\mu(E, z)} P_z + V_s(z) + V_{ext}(z)\ ]\ f = E\, f \tag{1.50}$$

where

$$\frac{1}{\mu(E, z)} = \frac{2p^2}{3} [\ \frac{2}{E + E_A - V_p - V_{ext}} + \frac{1}{E - E_A + \Delta_A - V_\delta - V_{ext}}\ ] \tag{1.51}$$

and μ is the effective mass, which depends on the position and energy.

We have now succeeded in the derivation of a Schrodinger-like equation for the envelope function, which is parametrized by effective parameters. To proceed we must derive some connection rules at the interfaces for the envelope function: boundary conditions.

2.3.4 Boundary Conditions

The differential system must be completed by boundary condition. Generally, for envelope functions the boundary conditions can be given by a continuity argument of envelope function.

Since the effective Hamiltonian is quadratic in p_z, the envelope function **f** should be continuous everywhere and in particular across the heterointerfaces.

Such a condition ensures that Eq.(1.28) is an acceptable quantum-mechanical function. The second rule(the equivalent of the $\frac{\partial \phi}{\partial z}$ continuity in vacuum) is fulfilled by demanding the continuity of **A·f**, where **A** is an 8 x 8 matrix with element A_{nm} equal to $\int D_{nn'} dz$. Since D is at most of the second-order in $\frac{\partial}{\partial z}$, **A** is at most of the first-order in $\frac{\partial}{\partial z}$. The continuity of **A·f** is the generalization for coupled bands of the well-known continuity condition of $\frac{\partial f}{\partial z}$, the derivative of a scalar wave function in one-dimensional quantum-mechanical problem. The continuity of **A·f** and not, say, of $\frac{\partial f}{\partial z}$, as could have been thought at first sight, is a boundary condition which warrants the conservation of the probability current, and ultimately the stationarity of the heterostructure wave function.

In addition, the long range behavior of **f** has to be specified. It depends on the problem under consideration. For bound states **f** should decay to zero at large z. For superlattices the spatial periodicities of $V_s(z)$, $V_p(z)$, $V_\xi(z)$ and $V_{ext}(z)$ lead to the Bloch theorem

$$f(z+d) = e^{iqd} f(z) \tag{1.52}$$

where d is the superlattice period and q is the superlattice wave vector that one may restrict to the first Brillouin zone of the superlattice

$$-\frac{\pi}{d} < q < \frac{\pi}{d} \tag{1.53}$$

When i) the in-plane wave vector $\mathbf{k}_\perp$ is equal to zero and ii) the coupling between light and heavy particle states are absent, an important simplification takes place: the boundary condition corresponding to Eqs.(1.50)-(1.51) is that

$$f, \ \frac{1}{\mu}\frac{\partial f}{\partial z} \text{ are continuous everywhere.} \tag{1.54}$$

CHAPTER 3
ANALYTICAL CALCULATIONS

3.1 Introduction

As mentioned in Chapter 2, the envelope function approximation is a useful method of describing the electronic-structure and optical properties of heterostructures. Generally, the solutions of the Schrodinger-like equations in which the properties of the hosts are presented in terms of effective parameters will provide all the information about the heterostructures. In this chapter we will give a general formalism for calculating the electronic-structure and transport properties of various polytype heterostructures.

The chapter is organized as following: In section 3.2, we demonstrate the transfer matrix method to solve the envelope function equations. Section 3.3 gives an explicit expression for calculating the tunneling coefficient, tunneling current and tunneling time through heterostructures. The subband structures of multiple quantum well and superlattice are presented in Section 3.4.

3.2 Transfer Matrix Approach

3.2.1 Basic Equation

In chapter two we have obtained the Schrodinger-like equation for envelope function in heterostructure. The equations with boundary conditions may be rewritten in the general forms

$$[\ P_z \frac{1}{2\mu(E,\ z)} P_z \ + V_s(z) \ + V_{ext}(z)\ ]\ f \ = E\, f \tag{3.1}$$

$$f \ \text{and} \ \frac{1}{\mu(E,\ z)} \frac{df}{dz} \ \text{continuie everywhere} \tag{3.2}$$

where $P_z = \frac{\hbar}{i}\frac{d}{dz}$,:, and $\mu(E, z)$ is the energy- and position-dependent effective mass:

(i) Effective Mass(one band) Model

$$\frac{1}{\mu(E, z)} = \frac{2p^2}{3}\left[\frac{2}{E_A - V_p} + \frac{1}{E_A + \Delta_A - V_\delta}\right] = \frac{1}{m^*_{\Gamma_6}} \tag{3.1a}$$

(ii) Two-band Model

$$\frac{1}{\mu(E, z)} = \frac{4p^2}{3}\left[\frac{1}{E + E_A - V_p - V_{ext}}\right] \tag{3.1b}$$

(iii) Three-band Model

$$\frac{1}{\mu(E, z)} = \frac{2p^2}{3}\left[\frac{2}{E + E_A - V_p - V_{ext}} + \frac{1}{E - E_A + \Delta_A - V_\delta - V_{ext}}\right] \tag{3.1c}$$

For studying the electronic structure and transition properties of heterostructures, and automatic solution matching at interfaces and ease of numerical computation, it is convenient to introduce the state vector

$$\mathbf{f}(z) = \begin{bmatrix} F_a(z) \\ \\ F_b(z) \end{bmatrix} \equiv \begin{bmatrix} f \\ \\ \frac{1}{\mu}\frac{df}{dz} \end{bmatrix} \tag{3.3}$$

whose components are continuous and satisfy the coupled equations

$$F'_a = \mu F_b \tag{3.4a}$$

$$F'_b = -\left[\frac{2(E - V_s - V_{ext})}{\hbar^2}\right] F_a \tag{3.4b}$$

consistent with Eq.(3.1)

Eq.(3.4) can also be written in the matrix form

$$\mathbf{f}' = \mathbf{A} \cdot \mathbf{f} \tag{3.5}$$

$$\begin{bmatrix} F'_a \\ F'_b \end{bmatrix} = \begin{bmatrix} 0 & \mu \\ -\gamma & 0 \end{bmatrix} \cdot \begin{bmatrix} F_a \\ F_b \end{bmatrix} \tag{3.5a}$$

and

$$\gamma = [\frac{2(E - V_s - V_{ext})}{\hbar^2}]$$

They, together with corresponding boundary conditions($\mathbf{f}$ are continuous everywhere), are the basic equations which can be solved easily by the transfer matrix approach.

3.2.2 Transfer Matrix

It is readily verified[30] that F(z) evolves according to

$$\mathbf{f}(z) = \mathbf{S}(z, z') \cdot \mathbf{f}(z') \tag{3.6}$$

with

$$\mathbf{S}(z, z') = \begin{bmatrix} F_a^{(1)} & F_a^{(2)} \\ F_b^{(1)} & F_b^{(2)} \end{bmatrix} \tag{3.7}$$

where $\mathbf{f}^{(1)}$ and $\mathbf{f}^{(2)}$ are particular solutions of Eq.(3.5) satisfying the initial conditions

$$\mathbf{f}^{(1)} = \begin{bmatrix} 1 \\ 0 \end{bmatrix}, \qquad \mathbf{f}^{(2)} = \begin{bmatrix} 0 \\ 1 \end{bmatrix}. \tag{3.8}$$

Eqs(3.6)-(3.8) give the definition of the transfer matrix and mean that state $\mathbf{f}(z')$ is transferred to state $\mathbf{f}(z)$ by the transfer matrix $\mathbf{S}(z, z')$. The transfer matrix $\mathbf{S}(z, z')$ has the following properties:

(a) As required by Eq.(3.6), $\mathbf{S}(z, z')$ reduces to the identity matrix when z = z':

$$\mathbf{S}(z, z')|_{z=z'} = I \; .$$

(b) Since the determinant of $\mathbf{S}(z, z')$ is the Wronskian of Eq.(3.4), then

$$\det \{ \mathbf{S}(z, z') \} = 1 \; ,$$

a necessary condition for particle conservation.

(c) inverse symmetry

$$\mathbf{S}(z', z) = \mathbf{S}^{-1}(z, z') \; .$$

Transfer Matrix for One Layer[0, L]

In a region [0, L], the transfer matrix $\mathbf{S}(z, z')$ is only determined by the parameters of this layer. Thus, $\mathbf{S}(L, 0)$ is the desired matrix for the layer, and equation

$$\mathbf{f}(L) = \mathbf{S}(L, 0) \cdot \mathbf{f}(0) \tag{3.9}$$

gives, if state $\mathbf{f}(0)$ is known, the state $\mathbf{f}(L)$.

Now let us form the transfer matrix $\mathbf{S}(z, z')$ in the layer. For the case: Vext(z) = 0 or constant within the layer, the Transfer matrix can easily be formed, by the general solutions of the equation (3.1) and the definition of transfer matrix, as following:

$$\mathbf{S}(z, z') = \begin{bmatrix} Cos\ k(z-z') & \frac{\mu}{k} Sin\ k(z-z') \\ -\frac{k}{\mu} Sin\ k(z-z') & Cos\ k(z-z') \end{bmatrix} \tag{3.10}$$

where

$$k^2 = \frac{2\mu\cdot\ (E-V_s)}{\hbar^2} \tag{3.11}$$

is the wave vector and uin is effective mass. Notice a) that $\det\{\mathbf{S}\} = 1$. b) $\mathbf{S}(z, z')$ is a real matrix no matter whether k is real or imaginary.

Transfer Matrix For Multiple Layers

Let us consider a multiple-layer heterostructure shown as Fig. 3.1.

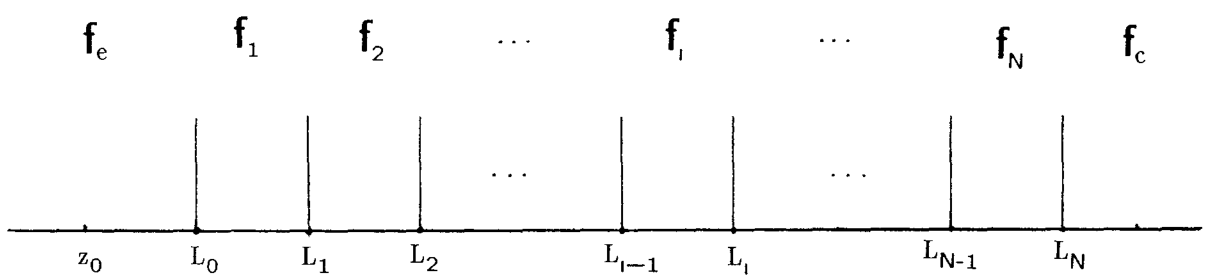

Figure 3.1 An N-layer Heterostructure

Within the ith layer, one may have

$$\mathbf{f}_i(L_i) = \mathbf{S}(L_i, L_{i-1})\cdot \mathbf{f}_i(L_{i-1}) \tag{3.12}$$

and at interfaces

$$\mathbf{f}_i(L_{i-1}) = \mathbf{f}_{i-1}(L_{i-1}) \tag{3.13}$$

required by continuity of $\mathbf{f}(z)$. Thus, combine these expressions, one may also find that

$$\begin{aligned}
\mathbf{f}_c(z) &= \mathbf{S}_c(z, L_N)\cdot \mathbf{f}_c(L_N) \\
&= \mathbf{S}_c(z, L_N)\cdot \mathbf{f}_N(L_N) \\
&= \mathbf{S}_c(z, L_N) \cdot \mathbf{S}_N(L_N, L_{N-1}) \cdot \mathbf{f}_{N-1}(L_{N-1}) \\
&\quad \cdots \\
&= \mathbf{S}_c(z, L_N) \cdot \mathbf{S}_N(L_N, L_{N-1}) \cdot \mathbf{S}_{N-1}(L_{N-1}, L_{N-2}) \cdots \\
&\qquad \mathbf{S}_2(L_2, L_1) \cdot \mathbf{S}_1(L_1, L_0) \cdot \mathbf{S}_e(L_0, z_0) \cdot \mathbf{f}_e(z_0) \\
&= \mathbf{S}_c(z, L_N) \cdot \mathbf{S}_{NLH}(L_N, L_0) \cdot \mathbf{S}_e(L_0, z_0) \cdot \mathbf{f}_e(z_0)
\end{aligned} \tag{3.14}$$

where

$$\begin{aligned}
\mathbf{S}_{NLH}(L_N, L_0) \equiv \mathbf{S}_N(L_N, L_{N-1}) \cdot \mathbf{S}_{N-1}(L_{N-1}, L_{N-2}) \cdots \\
\cdot \cdot \mathbf{S}_i(L_i, L_{i-1}) \cdots \mathbf{S}_2(L_2, L_1) \cdot \mathbf{S}_1(L_1, L_0)
\end{aligned} \tag{3.15}$$

is the transfer matrix of the multiple-layer heterostructure.

3.3 Tunneling

Suppose that a heterostructure consists of N layers[0, L]. Outside the heterostructure the wave function is given by

$$f(z) = \begin{cases} A_+ e^{\imath k_e z} + A_- e^{-\imath k_e z} & \text{for } z \leq 0 \\ B_+ e^{\imath k_c z} + B_- e^{-\imath k_c z} & \text{for } z \geq L , \end{cases} \tag{3.16}$$

where k_e, k_c define wave vectors in the respective regions. The corresponding state vectors are

$$\mathbf{f}_e(z) = \begin{bmatrix} 1 & 1 \\ \frac{\imath k_e}{\mu_e} & -\frac{\imath k_e}{\mu_e} \end{bmatrix} \begin{bmatrix} A_+ e^{\imath k_e z} \\ A_- e^{-\imath k_e z} \end{bmatrix} \tag{3.17}$$

and

$$\mathbf{f}_c(z) = \begin{bmatrix} 1 & 1 \\ \frac{\imath k_c}{\mu_c} & -\frac{\imath k_c}{\mu_c} \end{bmatrix} \begin{bmatrix} B_+ e^{\imath k_c z} \\ B_- e^{-\imath k_c z} \end{bmatrix} \tag{3.18}$$

According to Eq.(3.14), $\mathbf{f}_c(z)$ and $\mathbf{f}_e(z)$ are connected by the transfer matrix $\mathbf{S}_{e\text{-}c}(z, z_0)$:

$$\mathbf{S}_{e\text{-}c}(z, z_0) = \mathbf{S}_e(z, L) \cdot \mathbf{S}_{NLH}(L, 0) \cdot \mathbf{S}_e(0, z_0) , \tag{3.19}$$

where $\mathbf{S}_{NLH}$ is the transfer matrix within the heterostructure.

3.3.1 Tunneling Coefficient

To calculate the tunneling coefficient T_{tunnel} in the left- and right-contacts (see

Fig.3.2), it is convenient to let A+ = 1, A- = R, B+ = T and B- = 0 in Eq.(3.16). Then we get

$$f_e(z) = e^{\imath k_e z} + R\, e^{-\imath k_e z}, \qquad \text{for} \quad z \leq 0 \; ; \tag{3.19}$$

$$f_c(z) = T\, e^{\imath k_c z}, \qquad \text{for} \quad z \geq L \; . \tag{3.20}$$

where R, T are the reflection, and transmission amplitudes, and k_e, k_c the wave vectors in the emitter and collector respectively. The tunneling coefficient is defined as following:

$$T_{\text{tunnel}} = \frac{k_c \mu_e}{k_e \mu_c} \mid T \mid^2 \tag{3.21}$$

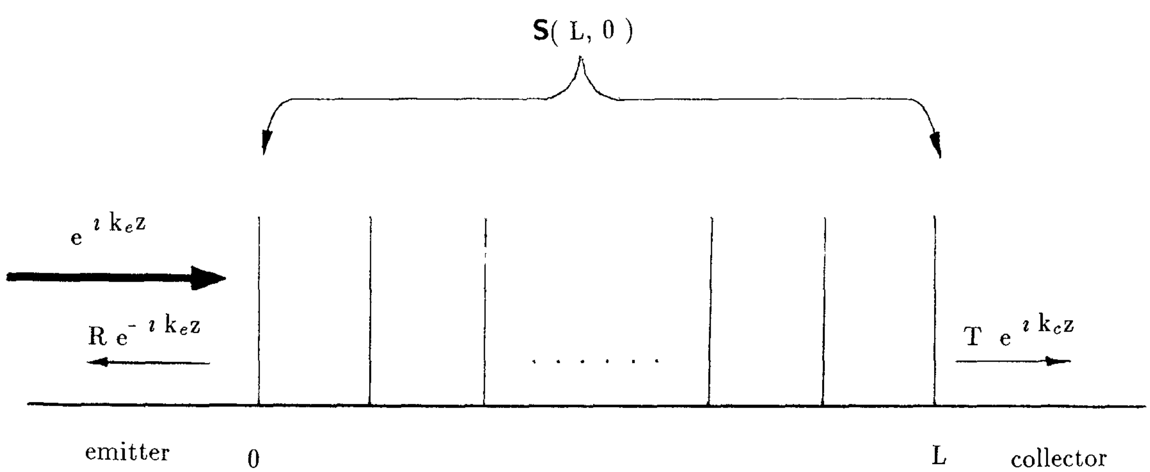

Figure 3.2 Tunneling in the Left- and Right- Contacts

To calculate T, we shall first find the relationship between T and the transfer matrix. After comparing Eqs.(3.19)-(3.20) with Eqs.(3.16)-(3.18), letting z = L, z'= 0, one may find

$$\begin{bmatrix} T e^{i k_c z} \\ 0 \end{bmatrix} = \mathbf{m} \cdot \begin{bmatrix} 1 \\ R \end{bmatrix} \tag{3.22}$$

where

$$\mathbf{m} = \begin{bmatrix} M_{11} & M_{12} \\ M_{21} & M_{22} \end{bmatrix}$$

$$= \frac{1}{2} \begin{bmatrix} 1 & \frac{\mu_c}{i k_c} \\ 1 & -\frac{\mu_c}{i k_c} \end{bmatrix} \cdot \mathbf{S}_{NLH}(L,\ 0) \cdot \begin{bmatrix} 1 & 1 \\ \frac{i k_e}{\mu_e} & -\frac{i k_e}{\mu_e} \end{bmatrix} \tag{3.23}$$

Thus the reflection and transmission amplitudes R and T are given by

$$R = -\frac{M_{21}}{M_{22}}, \qquad T = \frac{\det\{\mathbf{m}\}}{M_{22}} \tag{3.24}$$

From Eqs.(3.27)-(3.28) and the identity of the determinant of $\mathbf{S}(L, 0)$, we finally obtained the tunneling coefficient through an arbitrary heterostructure

$$T_{tunnel} = \frac{k_e \mu_c}{k_c \mu_e} \frac{1}{|M_{22}|^2}$$

$$= \frac{4}{2 + (\frac{k_c \mu_e}{k_e \mu_c})^2 S_{11}^2 + (\frac{k_e \mu_c}{k_c \mu_e})^2 S_{22}^2 + (\frac{k_e k_c}{\mu_c \mu_e})^2 S_{12}^2 + (\frac{\mu_e \mu_c}{k_c k_e})^2 S_{21}^2} \tag{3.25}$$

where Sij are the element of the transfer matrix $\mathbf{S}(L, 0)$ within the heterostructure.

It is noted that Eq.(3.29) gives the general expression for calculating the tunneling coefficient through an arbitrary multiple-layer heterostructure and is based on the envelope function approximation and correct boundary conditions. The formalism reduce to the well-known expression obtained by authors[2, 29] under different limits and simplifications.

3.3.2 Tunneling Current

To find the net tunneling current, we need to define the energy E which measures from the energy of the incident electron and E', that of the transmitted. The current density J may be computed as the average of the product of T_{tunnel} by the group velocity, $V(k) = \hbar \nabla_k E$

$$J = \langle e \, V(k) \, T_{tunnel} \rangle$$

$$= \frac{2e}{(2\pi)^3} \int dk \quad V(k) \, T_{tunnel} \, [f(E) - f(E')] \tag{3.26}$$

where $f(E) = [1 + exp(\frac{E-E_f}{k_B \theta})]^{-1}$ is the Fermi-Dirac distribution at absolute temperature θ, and with E_f being the Fermi energy and k_B the Boltzmann constant. Because of a separation of the variables, the tunneling coefficient T_{tunnel} is only a function of the longitudinal energy. It can be shown that the transverse components of J are zero by symmetry, and that, after changes of variable from momentum to energy, the longitudinal component becomes

$$J_z = \frac{2em^*}{(2\pi)^2\hbar^3} \int dE_l \int dE_t \; T_{tunnel} \; [f(E) - f(E')] \tag{3.27}$$

Integrating over the transverse energy, we find

$$J_z = \frac{2em^* k_B \theta}{(2\pi)^2 \hbar^3} \int_0^{\infty} dE_l \quad T_{tunnel} \quad Ln \left\{ \frac{1 + exp(\dfrac{E_f - E_l}{k_B \theta})}{1 + exp(\dfrac{E_f - E_l - V_a}{k_B \theta})} \right\} . \tag{3.28}$$

For $\theta \longrightarrow 0$, the above expression becomes

for $V_a \geq E_f$,

$$J_z = \frac{2em^*}{(2\pi)^2 \hbar^3} \int_0^{E_f} dE_l \quad T_{tunnel}\left(E_f - E_l\right) \quad ;$$

for $V_a \leq E_f$,

$$J_z = \frac{2em^*}{(2\pi)^2 \hbar^3} \left\{ V_a \int_0^{E_f} dE_l \quad T_{tunnel} \quad + \int_{E_f - V_a}^{E_f} dE_l \quad T_{tunnel}\left(E_f - E_l\right) \right\} \tag{3.29}$$

3.3.3 Tunneling Time

To a good approximation, the time it takes an electron tunnel out a bound quantum well state is given by[24]

$$\tau_t = \frac{t_c}{T_{tunnel}} \tag{3.30}$$

where

$$t_c = \frac{2\,W}{V_g} \tag{3.31}$$

is the classical oscillation period of the electron with the velocity V_g in the quantum well, and W the width of the quantum well (see Fig. 3.3) The tunneling time may be understood as semiclassical tunnel time which is the time to be taken by an electron completely tunneling through the barrier. Because during the period t_c only the

T_{tunnel} parts of an electron tunnel through the barrier.

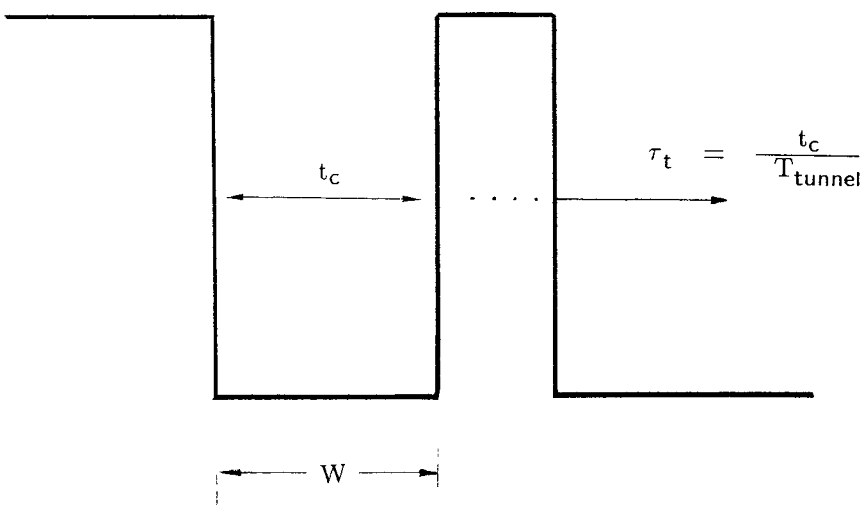

Figure 3.3 Tunneling time through a barrier

3.4 Subband Structures and States in Superlattices

3.4.1 Subband Structures

Consider a superlattice with the periodicity D. The periodicity of wave function implied the state vector $\mathbf{f}$ satisfies Bloch Theorem:

$$f(z + D) = e^{\pm \imath qD} f(z) \tag{3.32}$$

On the other hand,

$$\mathbf{f}(z + D) = \mathbf{S}_S(z + D, z) \cdot \mathbf{f}(z) \tag{3.33}$$

A combination of these gives

$$\left\{ \mathbf{S}_s(z + D z) - \lambda \ I \right\} \cdot \mathbf{f}(z) = 0 , \qquad \lambda = e^{\pm \imath qD} . \tag{3.34}$$

The condition for the equation to have a nontrivial solution is that the determinant of the coefficient vanish. Thus

$$\begin{vmatrix} S_{s11} - \lambda & S_{s12} \\ S_{s21} & S_{s22} - \lambda \end{vmatrix} = 0 \tag{3.35}$$

This gives an equation of the second degree for λ . The summation of the two roots of λ is

$$\lambda_1 + \lambda_2 = e^{\imath qD} + e^{-\imath qD} = S_{s11} + S_{s22} \tag{3.36}$$

and the dispersion relation of the superlattice becomes

$$2 \ Cos \ qD = S_{s11} + S_{s22} \tag{3.37}$$

3.4.2 Envelope State Functions

The superlattice envelope functions are the eigenstates in Eq.(3.34)). From this equation, one may easily find The ratio of $F_a(z_0)$ and $F_b(z_0)$ at an arbitrary point z_0

$$\frac{F_a(z_0)}{F_b(z_0)} = \frac{S_{s12}}{S_{s11} - \lambda} . \tag{3.38}$$

Therefore, the wave function at z can be constructed from an initial point z_o by

$$\mathbf{f}(z) = \mathbf{S}(z, z_0) \cdot \mathbf{f}(z_0)$$

$$= \mathbf{S}(z, z_0) \cdot \begin{bmatrix} \frac{S_{s12}}{S_{s11} - \lambda} \\ \\ 1 \end{bmatrix} \times \text{Constant} \tag{3.39}$$

where S_{s11}, S_{s12} are the elements of $\mathbf{S}_s(z + D, z)$ and $\mathbf{S}(z, z_0)$ is the transfer matrix from z_0 to z, the constant may be determined by the normalization. Note that, although there are two wave functions for $\lambda = e^{\pm \imath qD}$, their absolute values, i.e. the square roots of probabilities are equal.

3.5 Summary and Conclusion

In the chapter we have presented a general formalism for calculating the tunneling and subband structure in various types of quantum wells. The formalism is developed by combining the envelope function approximations theory and the transfer matrix techniques. It is very useful for the analysis of quantum wells and superlattices, and can be applied for device designing. The keys of the formalism are

1. By Introducing a state vector $\mathbf{f}(z) = [\, f, \ \frac{1}{\mu} \frac{df}{dz} \,]^{\top}$, the envelope function equation can be rewritten as

$$\mathbf{f}' = \mathbf{A} \cdot \mathbf{f}$$

2. The state vector $\mathbf{f}(z)$ evolves according to

$$\mathbf{f}(z) = \mathbf{S}(z, z') \cdot \mathbf{f}(z')$$

where $\mathbf{S}(z, z')$ is the transfer matrix.

3. The transfer matrix of a layer is formed by the solutions of the envelope function equation, depending on the structural and band parameters of the layer.
4. The transfer matrix of multiple layers is the simple products of the matrix of each layer.
5. Once known the transfer matrices of the quantum well structure, all information about the quantum well structure can in principle be calculated.

CHAPTER 4

APPLICATION TO THE FEASIBILITY STUDY OF QUANTUM-WELL INFRARED LASER

4.1 Introduction

In the chapter, as an application we apply the envelope function approach to the calculation of the subband structures and tunneling properties of a special designed quantum well structure, which may be a candidate for infrared laser. The analytical results of the previous chapter are implemented into computer simulations. The general considerations on the realization of lasing are presented in Section 4.2, where the necessary conditions to achieve population inversion in quantum well subband transition laser are discussed. The feasibility studies of multiple quantum well (MQW) far infrared Laser are presented in Section 4.4..

Fortran-77 was used to write a program for calculating the subband structures and tunneling coefficients of various polytype heterostructures. The program has been run in the VAX/VMS on node TESLA in NJIT.

4.2 General Considerations

Since the theoretical proposal of the generation and amplification of infrared light in a semiconductor superlattice, optical transitions between subbands in quantum well structures have received considerable attention.[21-26] One of the advantages of using quantum well structures is the possibility of tuning the wavelength corresponding to the intersuband transition energy by changing the barrier thickness and height as well as the well width and depth.

For the realization of lasing in quantum well structures, one of the important steps is to design situations where population inversion is possible. Another important step is to achieve the efficiency of the stimulated radiation.

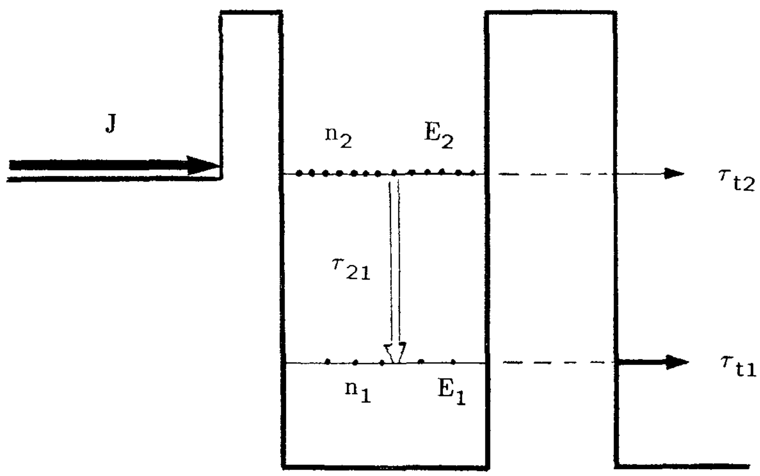

Figure 4.1 Schematic Structure Depicting the Basic Principles of Creating Population Inversion in Quantum Well Subbands by Current Injection.

Before discussing the structure and calculation results, it is instructive for later reference to discuss briefly the general model of lasing condition in quantum well structures (Fig. 4.1). A feature common to all the devices proposed is current injection by resonant tunneling from one side of the active layer to the upper subband, and resonant tunneling from the lower subband to the other side of the active layer. This feature can be described by the following set of simplified rate equations:

$$\frac{dn_2}{dt} = \frac{J}{e} - \frac{n_2}{\tau_{21}} - \frac{n_2}{\tau_{t2}} \qquad (4.1)$$

$$\frac{dn_1}{dt} = \frac{n_2}{\tau_{21}} - \frac{n_1}{\tau_{t1}} \qquad (4.2)$$

where n_1(n_2) is the electron density in subband 1(2) of the quantum well, J is the current density. It is clear that electrons injected into the subband 2 can either tunnel through the barrier with time τ_{t2} or relax to the lower subband 1 with relaxation time τ_{21}. In a steady-state condition one may easily find

$$n_2 = \frac{J}{e} \frac{1}{\left(\frac{1}{\tau_{21}} + \frac{1}{\tau_{t2}}\right)} \tag{4.3}$$

and

$$\frac{n_2}{n_1} = \frac{\tau_{21}}{\tau_{t1}} \tag{4.4}$$

Equation (4.3) and (4.4) imply that the population inversion is controlled by the condition

$$\tau_{21} \gg \tau_{t1} \tag{4.5}$$

while the electron concentration in the upper subband is determined by the tunneling density and the rate of relaxation under the condition

$$\tau_{t2} \gg \tau_{21} , \tag{4.6}$$

Thus, we conclude an appropriate combined requirement for realization of the population inversion:

$$\tau_{t2} \gg \tau_{21} \gg \tau_{t1} . \tag{4.7}$$

This requirement will play an important rule in the design of quantum well laser structures discussed in following sections.

4.3 Design Idea and Structure

To realize population inversion, it is required to remove electron from the lower subband faster than the tunneling time of the upper subband. It imply, when designed for a structure, that a tunneling inversion is necessary in the structure. As a first candidate[22], the resonant tunneling diode is naturally chosen. A structure of periodically repeated resonant tunneling diodes is shown in Fig.4.2. a single period of the structure consists of two undoped quantum wells defined by three barrier I, II, III.

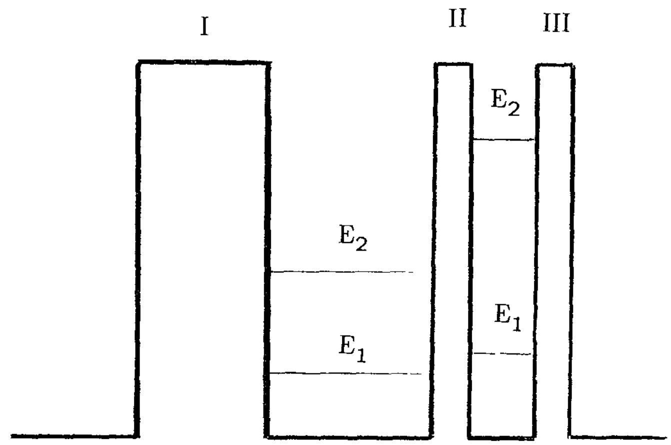

Figure 4.2 Structur-I: Double Quantum Well Resonant Tunneling Structure

However, for the structure, scattering and subband broadening are the serious problems which can strongly diminish the selectivity of the tunneling process[21].

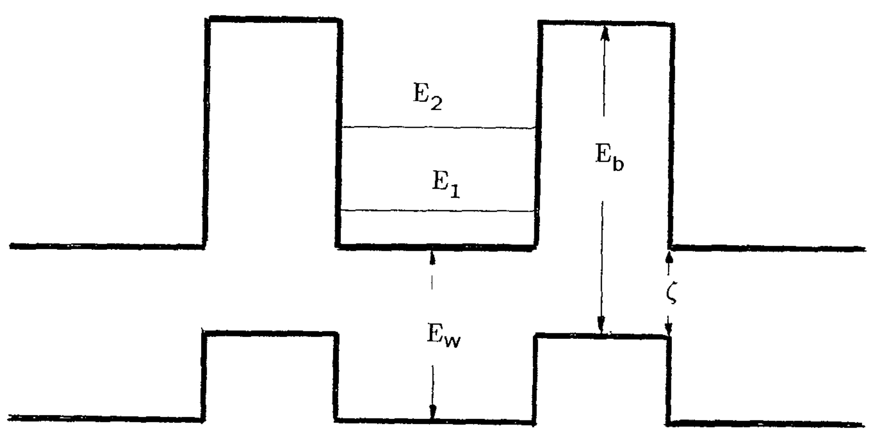

Figure 4.3 Structur-II: Schematic of the Band Alignment of a Type-II Heterostructure

Another possible structure is the tunneling diode composed of type-II heterojunctions[24]. Recently tunneling measurements have been performed in the type-II heterostructure (see Fig. 4.3), showing negative differential resistance upon tunneling through a single barrier[16, 17, 19]. This phenomena can be understood as inversion of the tunneling rate through the barrier by the theory of two-band model. In this model, the wave vector in the barrier can be express as

$$k^2 = \frac{3}{2\hbar^2 P^2}(E+\zeta)(E+\zeta-E_b)$$

where the zero of energy is measured from the conduction-band edge of the well material. For $-\zeta < E < E_b-\zeta$, k^2 becomes negative and k imaginary. If $|k| = \alpha$, α^{-1} corresponds to the penetration length of exponentially decaying waves in the barrier. The relationship between A and E shown in Fig. 4.4 imply that the inversion of tunneling rate take place in the range: $0 < E < \frac{E_b}{2} - \zeta$

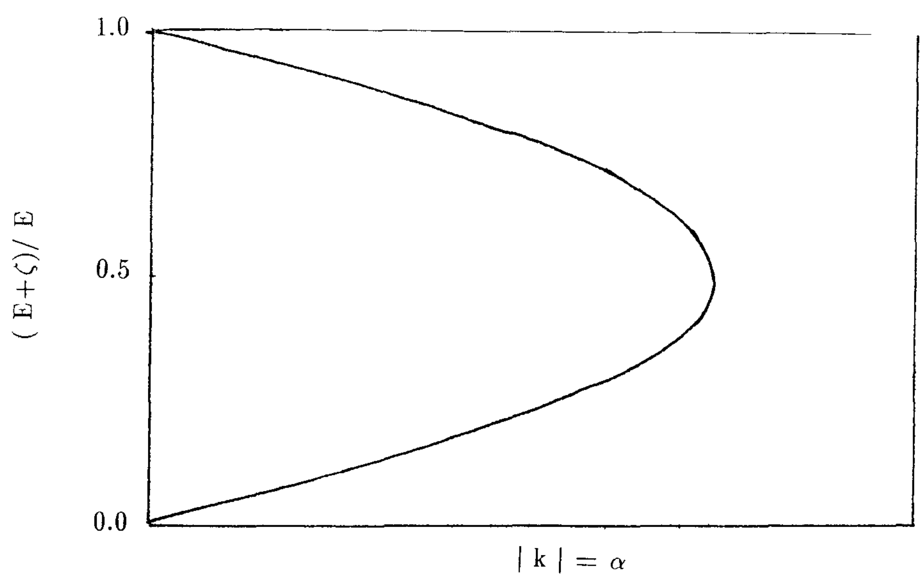

Figure 4.4 The Dispersion Relation in the Barrier

Fig. 4.5 gives the calculated tunneling coefficient as a function of energy, $T_{tunnel}(E)$, for different barrier thickness and two different band lineups. These results are close to those of M. Helm and S. J. Allen. Therefor, a negative conclusion is arrived in this structure.

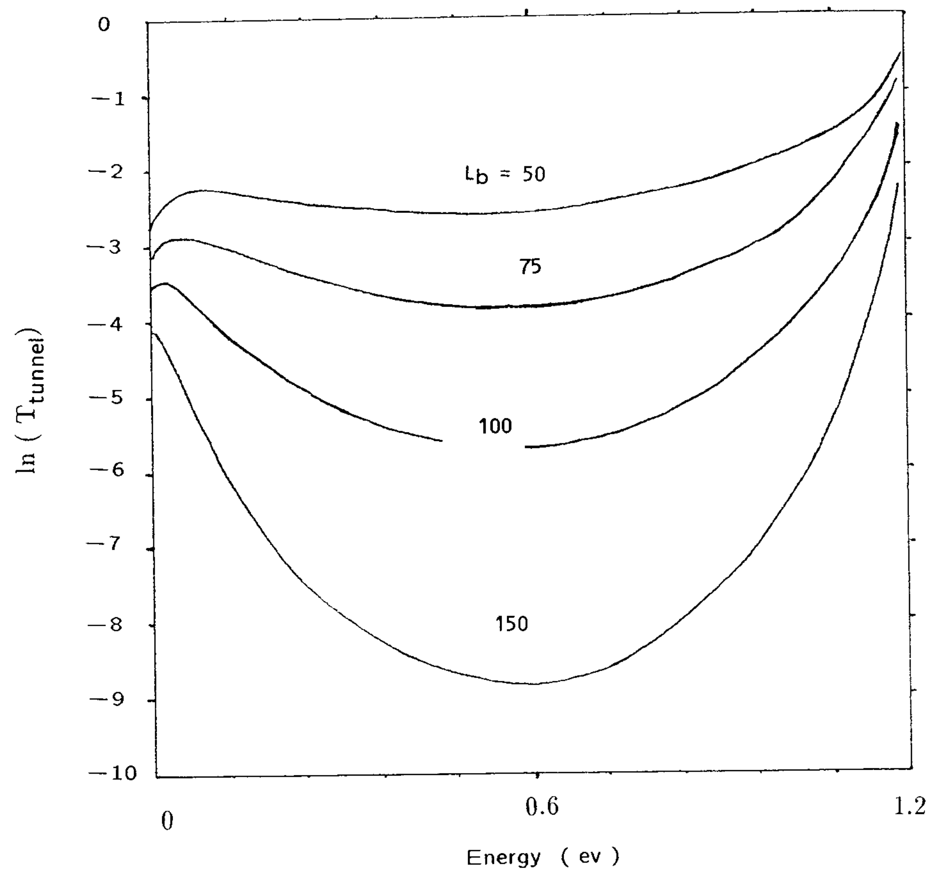

Figure 4.5 Calculated Tunneling Coefficients versus Energies for Structur-II

We have seen that, to achieve the population inversion the Structure-I take an advantage of resonant tunneling while Structure-II uses a type-II heterostructure to invert the tunneling probabilities. However, the selectivity of the tunneling process in former structure could be strongly diminished by an unavoidable nonresonant leakage current caused by scattering and level broadening, and the later structure also could not achieve the population inversion due to an insufficient negative slope of $T_{tunnel}(E)$ to satisfy the requirement of Eq.(4.6). In the following we present a structure and discuss its possibility and operation principle.

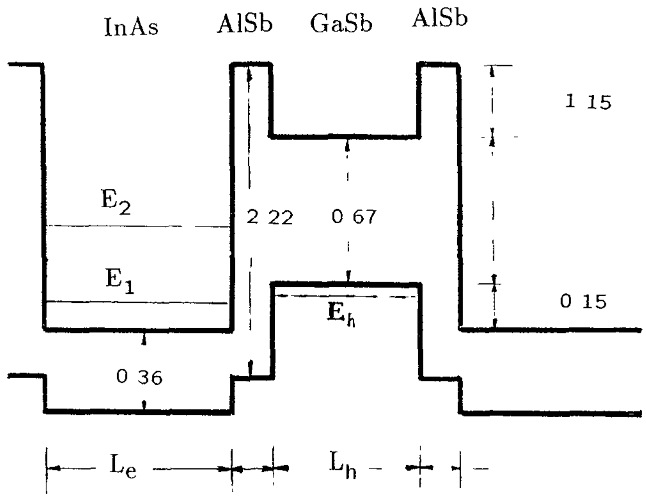

Figure 4.6 Structure-III: Schematic Band Diagram of a Polytype Heterostructure for the Realization of Population Inversionbetween the Electron Subbands in a Quantum Well

Structure-III shown in Fig. 4.6 may be a candidate for an infrared laser. It is a polytype heterostructure formed by type-I and type-II heterojunctions. The basic idea of the structure is to achieve population inversion through resonant interband tunneling which is a result of the existence of a tunneling window between the conduction band edge of InAs and the valence band edge of GaSb[27]. The idea also comes from the experimental results of a high peak-to-valley ratio in polytype GaSb/AlSb/InAs system done to date[16--20].

To achieve population inversion between subbands E_1 and E_2 the upper subband is pushed up into the forbidden gap of GaSb while the lower subband resides within the tunneling window. Thus the most likely path for electrons at E_2 is through a transition to E_1 and then from there tunneling into the well in the valence band of GaSb and finally reaching the adjacent layer. The purpose of having the well sandwiched between AlSb barriers is to enhance the effects of intersubband tunneling from subband E_1 and to reduce the tunneling rate related to E_2 The hole subband Eh is designed to be above E_1 such that it will move down to align up with

E_1 under a certain bias Vc. To realize these operation conditions, it is important to predicate the subband structures and tunneling properties (tunneling coefficients and tunneling times) by an accurate simulation of the structure.

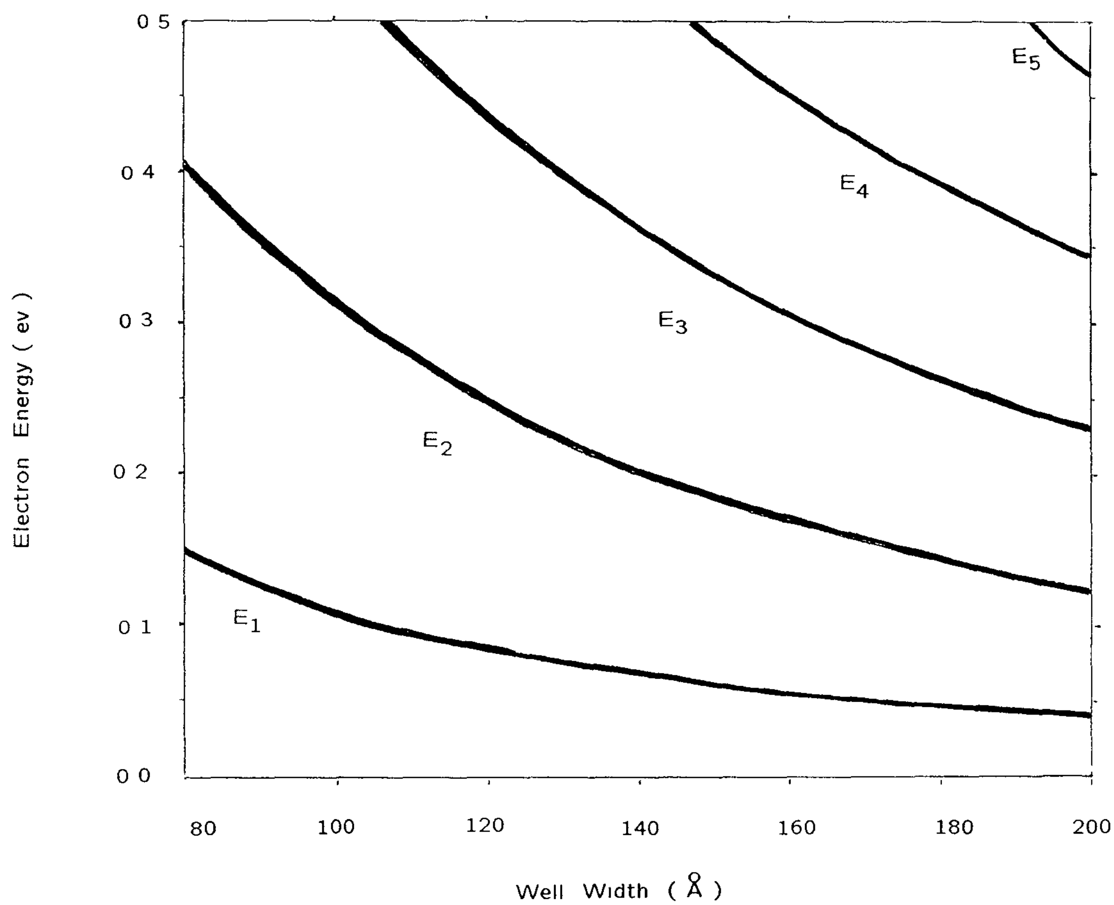

Figure 4.7 Calculated Subband Structures versus the Width of InAs Layer.

4.4 Numerical Results

Using the theoretical approach obtained in the previous chapter, we have calculated the subband structures, the tunneling coefficients, and tunneling times for the type of structures as shown in Fig. 4.6. From the calculations, we find that

(a) The electron subband location in InAs well is a strong function of the well width L_e (see Fig. 4.7). Similarly, the hole subband location in GaSb well is a strong function of the well width L_h. Therefore, by adjusting the well width, the wavelength of laser corresponding to the subband gap can be tuned.

(b) The barrier thickness of AlSb controls the peak-width of resonant tunneling through the window. The thicker the barriers are, the narrower the peak-width of tunneling becomes. This can be understood as a broadening of the hole subband due to the correlation of the state between adjacent wells.

(c) The GaSb layer serves as either a barrier to electrons at E_2 or a tunneling window to electrons at E_1. To greatly invert the tunneling rate, the GaSb layer should be wider. However, the width of GaSb layer is limited by the appropriately positioning of the resonant subband in the window for the practical design.

(d) The key of the structure is that it can provide a sufficient negative slope of $T_{tunnel}(E)$ while the $T_{tunnel}(E)$ of lower subband is close to unity. this effect means that, in contrast to Structure-II, the two physical requirements of both inverted and fast tunneling rates can be fulfilled simultaneously in the structure.

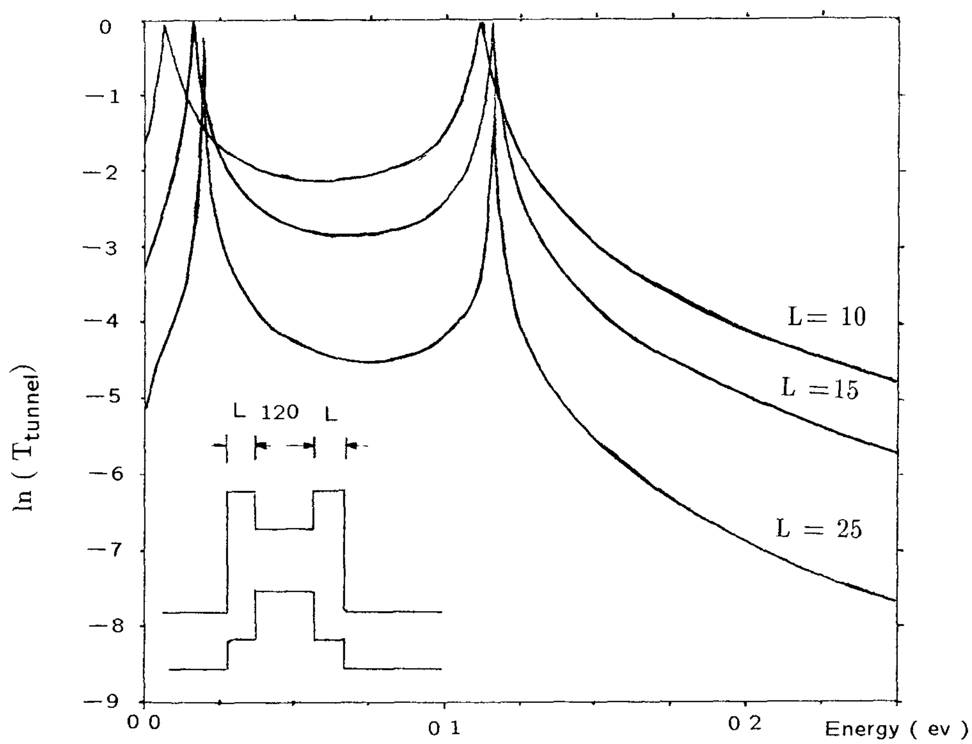

Figure 4.7 Tunneling Coefficients versus Energies

4.5 Discussions and Conclusions

Now let us discuss the possibilities of population inversion for the structure operating in two typical wavelengths of 10μm and 40μm.

Relaxation Time in InAs Quantum Well[21, 22, 24, 25]

It is an important input parameter for considerations of population inversion here. It depends on the material and temperature, and can be determined by the experiments of optical- and acoustic-phonon emission rates. For the case of $\Delta E = E_2 - E_1$ larger than the LO-phonon energy, E_{op}(e. g., 35 mev for GaAs), the relaxation time is dominantly determined by the process of LO-phonon relaxation (having a characteristic time $\tau_{21} \sim 10^{-12}$ s)[21, 23, 24, 25]. For the subband separations smaller than LO-phonon energy E_{op}, both LA-phonon relaxation and Auger process are expected to be the dominant mechanism for intersubband transitions, giving a characteristic time $\tau_{21} \sim 10^{-10}$ s. Because of the lack of sufficient experimental data on intersubband relaxation time in InAs quantum wells, we use value for InGaAs as an estimate. For InGaAs quantum wells experiment gives a upper limit of $\tau_{21} = 3$ (ps) for $\lambda = 10\ \mu$m and $\tau_{21} = 600$ (ps) for $\lambda = 40\ \mu$m . It is reasonable to expect that in InAs quantum well τ_{21} will be even large, because of smaller electron effective mass and lower electron-phonon coupling in this material. However, we use a conservative value of $\tau_{21} = 1$ (ps) for $\lambda = 10\ \mu$m , and $\tau_{21} = 500$ (ps) for $\lambda \geq 40\ \mu$m .

Tunneling Times from Subbands

They depend on the values of the tunneling coefficients of related subbands. The tunneling time of lower subband, τ_{t1} , controls the population inversion while the tunneling time τ_{t2} determines the density residing in the upper subband. The calculated tunneling coefficients versus energies are shown in Fig. 4.8.

The calculated results of the structure are listed in table 4.1 for two possible structures operating at 10 um and 40 um. From the calculations, we find that

(1) For a moderate current density of J = 10^4 (A/cm^2), population inversions of $n_2 - n_1 = 5\ 10^{10}$ (cm^{-2}) and $n_2 - n_1 = 3.1\ 10^{13}$ (cm^{-2}) can be achieved for $\lambda = 10\ \mu m$ and $\lambda = 40\ \mu m$, respectively.

Table 4.1 Calculated Parameters of the InAs/AlSb/GaSb Polytype Structure

λ (μm)	10	10	40
L_e (Å)	150	150	400
L_h (Å)	120	120	120
L (Å)	15	10	25
E_1 (ev)	0.061	0.060	0.01
E_2 (ev)	0.185	0.185	0.04
E_h (ev)	0.115	0.113	0.116
τ_{21} (ps)	1	1	500
τ_{t1} (ps)	0.4	0.1	21
τ_{t2} (ps)	$1\ 5\times10^4$	1.5×10^3	3×10^4
n_2-n_1 (cm^{-2})	3.7×10^{10}	5.0×10^{10}	3.1×10^{13}

(2) The relaxation time is the key limit of realization of population inversion. The characteristic time τ_{21} in the picosecond range is a serious limit in all efforts to achieve population inversion for a laser of $10\ \mu m$, which is a strong desire for many significant applications. It is difficult to design a subband laser structure in which the tunneling time of lower subband is less than 1 (ps) and at the same time a sufficient large inverted rate of tunneling is achieved. It may be a right reason that the development of intersubband laser of 10 um is a rather difficult task.

(3) It should be noted that this design has established a fundamental step--a

possible population inversion--towards the realization of an intersubband laser. To design a practical laser, a much greater effort must be made. As an immediate next step one should calculate the optical gain coefficient and laser efficiency taking into account the device geometry and all possible optical loses. In my view, the feasibility study of infrared intersubband laser is a very interesting topic. I look forward to experiments and theoretical modeling to ascertain whether the intersubband Infrared lasing can be achieved.

In summary, based on the calculations of subband structures and tunneling, we have presented a quantum well device based on InAs/AlSb/GaSb polytype heterostructures in which population inversion between subbands can be achieved. Infrared emission in the device is therefore possible under a forward bias condition. For a moderate current injection of 10^4 (A/cm^2), the population inversion could be as high as 5×10^{10} ---3.1×10^{13} (cm^{-2}).

BIBLIOGRAPHY

[1] Kane, E. O. "Band Structure of Indium Antimonide." *J. Phys. Chem. Solid* 1 (1957):249-261.

[2] Tsu, R., and L. Esaki. "Tunneling in a Finite Superlattice." *Appl. Phys. Lett.* 22 (1973):562-564.

[3] Esaki, L. "A Bird's-Eye View on the Evolution of Semiconductor Superlattice and Quantum Wells." *IEEE QE*-22 (1986): 1611-1624.

[4] Bastard, G. "Theoretical Investigations of Superlattice Band Structure in the Envelope Function Approximation." *Phys. Rev.* B 25 (1981): 7584-7597.

[5] Bastard, G., and J. A. Brum. "Electronic States in Semiconductor Hetero-Structures." *IEEE QE*-22 (1986): 1625-1644.

[6] Altarelli, M. "Electronic Structure and Semiconductor-Semimetal Transition in InAs-GaSb Superlattices." *Phys. Rev.* B 28 (1983): 842-845.

[7] Cho, H. S., and P. R. Prucnal. "New Formalism of the Kronig-Penney Model with Application to Superlattices." *Phys. Rev.* B 36 (1987): 3237-3242.

[8] Schuurmans, M. F. H., and G. W. t'Hooft. "Simple Calculations of Confinement States in a Quantum Well." *Phys. Rev* B 31 (1984): 88047.

[9] Wang, K. L., and P. F. Yu. "Theory and Applications of Band-Aliged Superlattices." *IEEE QE*-25 (1989): 12-19.

[10] Cuypers, T. P., and W. Van Haeringen. "On the Theory of Envelope Function in Lattice-Matched Heterostructures." *Physica* B 168 (1990): 58-66.

[11] Hickmott, T. W., and P. M. Solomon. "Negative Charge, Barrier Heights, and the Conduction-Band Discontinuity in AlxGa1-xAs Capacitors." *J. Appl. Phys.* 57 (1984): 2844-2853.

[12] Dawson, P., B. A. Wilson, C. W. Tu and R. C. Miller. "Staggered Band Alignments in AlGaAs Heterojunctions and the Determination of Valence-Band Offsets." *Appl. Phys. Lett.* 48 (1986): 541-543.

[13] Wang, W. I., E. E. Mendez and F. Stern. "High Mobility Hole Gas and Valence-Band Offset in Modulation-Doped p-AlGaAs/GaAs Heterojunctions." *Appl. Phys. Lett.* 45 (1984): 639-640.

[14] Jogai, B., and K. L. Wang. "Dependence of Tunneling Current on Structural Variations of Superlattice Devices." *Appl. Phys. Lett.* 46 (1984): 167-168.

[15] Gerard, J. M., and J. Y. Marzin. "Direct Probing of Type-II Band Configurations in Semiconductor Superlattices." *Phys. Rev.* B 40 (1988): 6 450- 6453.

[16] Beresford, R., L. F. Luo and W. I. Wang. "Negative Differential Resistance in AlGaSb/InAs Single-Barrier Heterostructures at Room Temperature." *Appl. Phys. Lett.* 54 (1989): 2023-2025.

[17] Soderstrom, J. R., D. H. Chow and T. C. McGill. "Demonstration of Large Peak-to-Valley Current Ratios in InAs/AlGaSb/InAs Single-Barrier Heterostructures." *Appl. Phys. Lett.* 55 (1989): 1348-1350.

[18] Hermans, J., D. L. Partin and P. D. Dresselhaus. "Tunneling through Narrow-Gap Semiconductor Barriers." *Appl. Phys. Lett.* 48 (1986): 644-646.

[19] Miles, R. H., D. H. chow, J. N. Schulman and T. C. McGill. "Infrared Optical Characterization of InAs/Ga1-xInxSb Superlattices." *Appl. Phys. Lett.* 57 (1990): 801-803.

[20] Sweeny, M., and J. M. Xu. "Resonant Interband Tunnel Diodes." *Appl. Phys. Lett.* 54 (1988): 546-548.

[21] Helm, M., P. England, E. Colas, F. DeRosa and S. J. Allen. "Intersubband Emission from Semiconductor Superlattices Excited by Sequential Resonant Tunneling." *Phys. Rev. Lett.* 63 (1989): 74-79.

[22] Kastalsky, A., V. J. Goldman, J. H. Abeles. "Magnetic Field-Induced Suppression of Acoustic Phonon Emission in a Superlattice." *Appl. Phys. Lett.* 59 (1991): 2636-2638.

[23] Yang, R. Q., and J. M. Xu. "Population Inversion through Resonant Interband Tunneling." *Appl. Phys. Lett.* 59 (1991): 181-182.

[24] Helm, M., and S. J. Allen. "Can Barriers with Inverted Tunneling Rates Lead to Subband Population Inversion?" *Appl. Phys. Lett.* 56 (1990): 1366-1368.

[25] Borenstain, S., and J. Katz. "Intersubband Auger Recombination and Population Inversion in Quantum-Well Subbands." *Phys. Rev.* B 39 (1989): 10852-10857.

[26] Kastalsky, A., and A. L. Efros. "Possibility of Infrared Laser in a Resonant Tunneling Structure." *J. Appl. Phys.* 69 (1991): 841-845.

[27] Sai-Halasz, G. A., L. Esaki and W. A. Harrison. "InAs-GaSb Superlattice Energy Structure and Its Semiconductor-Semimetal Transition." *Phys. Rev.* B (1978): 2812-2818.

[28] Bauerle, R. T., T. Elsaesser, W. Kaiser, H. Lobentanzer, W. Stolz and K. Ploog. "Picosecond Infrared Spectroscopy of Hot Carriers in a Modulation-Doped $Ga_{0.47}In_{0.53}As$ Multiple-Quantum-Well Structure." *Phys. Rev.* B 38 (1988): 4307-4310.

[29] Vassell, M. O., J. Lee, and H. F. Lockwood. "Multibarrier Tunneling in Ga1-xAlxAs/GaAs Heterostructures." *J. Appl. Phys.* 54 (1983): 5206-5213.

[30] Swisher, G. M., " Introduction to Linear Systems Analysis." Wiley, New York (1985): 350-437.